ARTICLES

Dynamics of the O(^{3}P) + CS$_2$(X$^1\Sigma_g{}^+$) → SO(X$^3\Sigma^-$) + CS(X$^1\Sigma^+$) Reaction

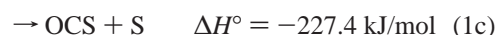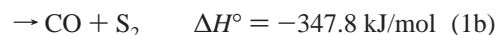**Yuying Cheng, Jiande Han, Xirong Chen, Yasuyuki Ishikawa, and Brad R. Weiner***

Department of Chemistry and Chemical Physics Program, University of Puerto Rico, P. O. Box 23346, University Station, Rio Piedras, Puerto Rico 00931

The rovibrational state distributions of both the CS and the SO products following the reaction of O(^{3}P) + CS$_2$ have been investigated. The O(^{3}P) atoms are generated by photolysis of NO$_2$ using a frequency-tripled Nd:YAG laser at 355 nm. The SO(X$^3\Sigma^-$, $v'' = 0-6$) and CS(X$^1\Sigma^+$, $v'' = 0-3$) are observed directly using laser induced fluorescence (LIF) spectroscopy on the (B$^3\Sigma^-$ − X$^3\Sigma^-$) and (A$^1\Pi$ − X$^1\Sigma^+$) transitions, respectively. The SO(X$^3\Sigma^-$) product is found to be highly excited with the vibrational state distribution inverted at $v'' = 1$ and detectable population up to $v'' = 6$, while the CS(X$^1\Sigma^+$) product vibrational state distribution is characterized as Boltzmann with a vibrational temperature of 1230 ± 155 K. The total vibrational excitation of both products accounts for 21% of the available energy to the products. The near nascent SO(X$^3\Sigma^-$, $v'' = 0-4$) rotational state distributions are characterized by rotational temperatures in the range of 882−1312 K, and the near nascent CS(X$^3\Sigma^+$, $v'' = 0$) is characterized by a temperature of 2986 ± 607 K. The total rotational energy of the products accounts for 34.8% of the available energy. Correlated ab initio calculations of the reaction pathway have been performed, resulting in accurate energies for the reactants, products, intermediates, and transition states. Optimized geometries for the intermediates and transition states have been obtained. The inverted vibrational state distribution of the SO(X$^3\Sigma^-$) product and the excited rotational state distribution of the CS(X$^1\Sigma^+$) product suggest a short-lived, nonlinear intermediate structure as the primary pathway for the reaction. The results from the ab initio calculations corroborate this model.

I. Introduction

The reactions of atomic oxygen play a fundamental role in basic chemical kinetics and dynamics and are of relevance in practical applications in atmospheric and combustion chemistry.[1−3] In particular, the oxidation reactions of small sulfur compounds, such as OCS, CS$_2$, and H$_2$S by oxygen atoms play an important role in the global sulfur cycle. These reactions can produce SO radicals that lead to SO$_2$ and ultimately yield acid rain in the atmosphere.[4] Oxygen atom reactions with sulfur species are also crucial in the combustion chemistry of sulfur-containing fuels.[5] For these reasons, many previous studies have been devoted to the kinetics of ground-state oxygen atom O(^{3}P), as well as its first excited state, O(^{1}D), reactions.[6] However, much less information is available about the microscopic dynamics of these reactions. Detailed dynamic studies have proven useful in unraveling ambiguous experiments, providing useful data to modelers.

The reaction of ground state oxygen atoms with carbon disulfide is a particularly interesting test case. Three product channels have been observed experimentally:[7]

$$O(^3P) + CS_2 \rightarrow CS + SO \qquad \Delta H° = -80.7 \text{ kJ/mol} \quad (1a)$$
$$\rightarrow CO + S_2 \qquad \Delta H° = -347.8 \text{ kJ/mol} \quad (1b)$$
$$\rightarrow OCS + S \qquad \Delta H° = -227.4 \text{ kJ/mol} \quad (1c)$$

Kinetic studies indicate that reaction 1a is the dominant pathway. The branching ratio of reaction 1c has been measured in the range of 0.015[8] to 0.3,[9] with the values converging toward 8−10%,[7,10] while reaction 1b has been reported from 0.014[11] to 0.03.[7] These product branching ratio studies suggest that the primary channel is reaction 1a, contributing approximately 90% of the total reaction rate.

Measurement of the temperature-dependent kinetics to obtain Arrhenius parameters was consistent with the branching ratio studies. Westenberg et al. used electron spin resonance spectroscopy to monitor the O(^{3}P) decay rates in the presence of CS$_2$ at three different temperatures.[12] They detected the SO(X$^3\Sigma^-$) to confirm the reaction and obtained an activation energy, $E_a = 1050$ cal/mol, for the process. A later study by Wei et al. is consistent with the first study, reporting an $E_a = 1280$ cal/mol for reaction 1 over the temperature range of 218−293 K.[13] Both of these groups used the same methodology to study the O(^{3}P) + OCS system and found equally consistent results.

Despite the wealth of kinetic and branching ratio data for reaction 1, there is relatively little information about the detailed dynamics of this system. This is particularly surprising in light of the fact that the O(^{3}P) + CS$_2$ was one of the earliest systems

---

* To whom correspondence should be addressed.

3694 *J. Phys. Chem. A, Vol. 105, No. 15, 2001*

Cheng et al.

studied by modern molecular dynamics methods. Smith used this system to demonstrate an elegant early example of product energy disposal as a mechanistic tool.[14] He photolyzed a mixture of NO_2 and CS_2 at $\lambda > 300$ nm and monitored the CS and SO products by transient absorption spectroscopy. The resulting CS and SO vibrational state distributions revealed vibrational temperatures of 1775 and 2870 K, respectively.

Reaction 1 was also the target of the early studies of reactive scattering in crossed molecular beams.[15,16] A more recent crossed beam investigation was undertaken in conjunction with experiments on the $O(^3P) + OCS$ system.[17] These studies have consistently found that the reaction is characterized by strong forward scattering and relatively low efficiency conversion of reaction exoergicity into translational energy. Because of the inefficiency of producing translational energy, the remaining exoergicity must be partitioned into the internal degrees of freedom of the reaction products. For this reason, energy partitioning studies into the primary channel, reaction 1a, provide an excellent test case for determining the detailed reaction mechanism.

We report here our studies into the rovibrational state distributions of both the CS and the SO reaction products following the 355 nm photolysis of NO_2 in the presence of CS_2. The $SO(X^3\Sigma^-, v'' = 0-6)$ and $CS(X^1\Sigma^-, v'' = 0-3)$ were observed directly using laser induced fluorescence (LIF) spectroscopy on the $(B^3E - X^3\Sigma^-)$ and $(A^1\Pi - X^1\Sigma^+)$ transitions, respectively. As a complement to the experimental work, we have carried out correlated ab initio calculations on the reaction pathway. The internal energy distributions of the reaction products, in conjunction with the results of the ab initio calculations, enable a complete description of the dynamics of the title reaction.

II. Methodology

Experimental. The experimental apparatus used in this study has been described previously.[18-20] In brief, atomic oxygen, $O(^3P)$, was generated by photolysis of NO_2 using the 355 nm output of a frequency-tripled Nd:YAG laser (Continuum, PL7000). The gases, CS_2 and NO_2, are introduced into a stainless steel reaction chamber through two inlets. The stainless steel chamber is equipped with extension arms to reduce scattered light. The partial and total pressures are measured at the exit of the chamber by a calibrated capacitance manometer. The probe dye laser (Lambda Physik FL3002; 0.25 cm^{-1} resolution) is pumped by a XeCl excimer laser operating at 308 nm. The two laser beams, photolysis and probe dye, are collinearly counter propagated along the entire length of the cell to ensure maximum overlap in the center of the reaction chamber.

The sulfur monoxide product is monitored by LIF on the $B^3\Sigma^- - X^3\Sigma^-$ transition in the 237−285 nm region with measurements of the vibrational state population distribution up to $v'' = 6$. The carbon monosulfide product is monitored by LIF on the $A^1\Pi - X^1\Sigma^-$ transition in the 244−270 nm region with measurements of vibrational state population distribution up to $v'' = 3$. In the case of both products, the vibronic bands are at least partially rotationally resolved. The probe wavelengths in the experimental region are generated by frequency doubling (β-BaB$_2$O$_4$) the dye laser fundamental outputs using three dyes (Coumarin 480, 500, and 540A). The probe laser powers (0.5−1.0 mJ) used in these experiments are not sufficient to saturate the observed transitions. No variation in rotational state distributions were observed as a function of dye laser power for several selected vibronic bands. Fluorescence is viewed at 90° relative to the laser beam axis by a high gain photomultiplier tube
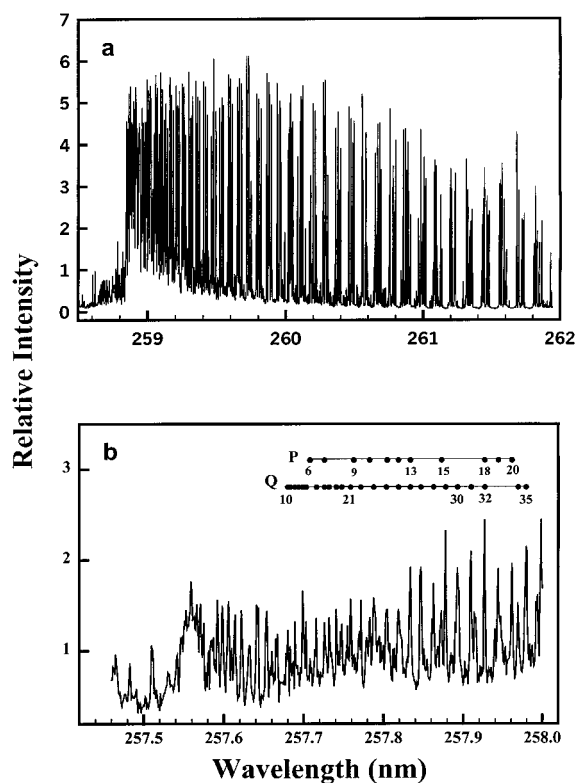

Figure 1. Rotationally resolved LIF spectra of (a) $SO(B^3\Sigma^-, v' = 1 - X^3\Sigma^-, v'' = 3)$ transition following 1.5 hard sphere collisions between $O(^3P)+CS_2$; (b) $CS(A^1\Pi, v' = 0 - X^1\Sigma^+, v'' = 0)$ transition following two hard sphere collisions between $O(^3P) + CS_2$.

(PMT). Long-pass filters were placed in front of the PMT to minimize the scattered light from photolysis and probe lasers. The output of the PMT is processed by a gated integrator and digitizer and sent to a computer for display and storage. The delay time (1−10 μs) between photolysis and probe lasers is controlled by a digital delay pulse generator.

Carbon disulfide and nitrogen dioxide were mixed in the reaction cell in a ratio of 0.8−0.9 at total pressures of 80−170 mTorr. CS_2 was degassed by three freeze−pump−thaw cycles before use; NO_2 (98%) was used without further purification. Both CS_2 and NO_2 were obtained commercially.

Theoretical Calculations. Ab initio calculations were carried out by the Gaussian 94 suite of computer programs.[21] Equilibrium geometries of the *trans-* and *cis*-OSCS intermediates and a set of harmonic frequencies for each structure associated with a minimum on the ground $^3A''$ potential energy surface are determined by second-order Moller−Plesset perturbation theory and the 6-311++G* basis set. Accurate energies for reactants, products, and the calculated intermediate and transition structures were determined by fourth-order Moller−Plesset theory (MP4 SDTQ/6−311++G*) and modified by a number of corrections to take into account further G-2 theoretical refinements.[22,23] The procedure includes a zero-point correction ΔE(ZPE) calculated from the harmonic frequencies. The second correction term, ΔE(2df), takes account of higher polarization functions on non-hydrogen atoms. This is done by comparing MP4 results with the 6-31 1++G*(2df) and 6-311++G* basis sets. The third correction, ΔE(QCI), is to perform a quadratic configuration interaction QCISD(T) calculations, using the 6-311++G* basis. Another higher level correction, ΔE(HLC), is added to the total electronic energy E_e. In G2 theory, a correction (Δ) is added to the energy, which accounts for the addition of a third d function to the non-hydrogen atoms. The

Dynamics of the O(^{3}P) + CS$_2$(X$^1\Sigma_g^+$) Reaction

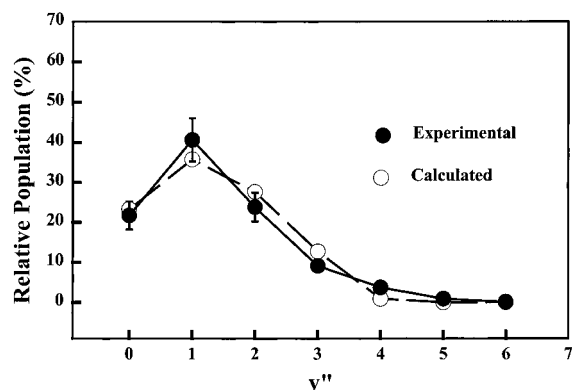*J. Phys. Chem. A, Vol. 105, No. 15, 2001* **3695**

Figure 2. Observed vibrational state distribution of the SO(X$^3\Sigma^-$) product (●) following the reaction of O(^{3}P) + CS$_2$. O(^{3}P) atoms are produced by the 355 nm photolysis of NO$_2$ (0.035 Torr) in the presence of CS$_2$ (0.04 Torr). The delay between the photolysis and the probe lasers is 2 μs, corresponding to 1.5 hard sphere collisions. The open symbols (○) and dashed line represents the best fit to the experimentally observed data using the Franck−Condon/Golden Rule model (see Discussion).

last term in the correction is 1.14npair, where npair is the number of valence pairs; the value of 1.14 was determined to give the zero mean deviation from the experiment of the calculated atomization energies of 55 molecules for which the experimental values are well-determined.

III. Results

A. Product Vibrational State Distributions. The vibrational state population distributions of the products SO(X$^3\Sigma^-$) and CS(X$^1\Sigma^-$) formed in the reaction of O(^{3}P) + CS$_2$ have been determined by using LIF excitation spectroscopy on the SO(B$^3\Sigma^-$ − X$^3\Sigma^-$) and CS(A$^1\Pi$ − X$^1\Sigma^+$) transitions (see Figure 1), respectively. Vibrational state distributions of SO(X$^3\Sigma^-$) have been successfully measured for a variety of unimolecular and bimolecular reactions in our laboratory.[18−20,24] For carbon monosulfide, we have calibrated our system by carrying out the 193 nm photodissociation of CS$_2$ and comparing the subsequent vibrational state distribution of CS with previous measurements.[25−27] The details of the vibrational state distribution measurement of each of the two products is given below.

1. SO(X$^3\Sigma^-$). For the SO(B$^3\Sigma^-$, v' − X$^3\Sigma^-$, v'') transition, the vibrational bands terminating on the $v' = 1$ level of the B$^3\Sigma^-$ state ($v' = 1$, $v'' = 0-6$) were used to determine the product vibrational distributions. Vibronic bands were assigned by using the spectroscopic constants reported by Colin.[28,29] The vibrational population distribution of SO(X$^3\Sigma^-$, $v'' = 0-6$) has been obtained by measuring the integrated areas of these bands and normalizing them by their respective Franck−Condon factors.[30] In these experiments, partial pressures of $P_{CS_2} = 40$ mTorr and $P_{NO_2} = 35$ mTorr and a delay time of 2 μs between the photolysis and probe lasers are used to obtain the SO spectra. Under these conditions ∼1.5 hard sphere collisions occur prior to detection of the LIF signal. The SO(X$^3\Sigma^-$) vibrational state population distribution measured under these conditions (see Figure 2) is not expected to undergo significant relaxation from its nascent partitioning.[31] As shown in Figure 2, the observed vibrational state distribution is inverted at $v'' = 1$ with detectable population up to $v'' = 6$.

2. CS(X$^1\Sigma^+$). Since vibrational state distributions of CS had not been previously measured in our laboratory, we recorded an LIF excitation spectrum of the CS(A$^1\Pi$ − X$^1\Sigma^+$) transition following the 193 nm photodissociation of CS$_2$. The vibronic bands of the CS(A$^1\Pi$ − X$^1\Sigma^+$) transition were assigned using
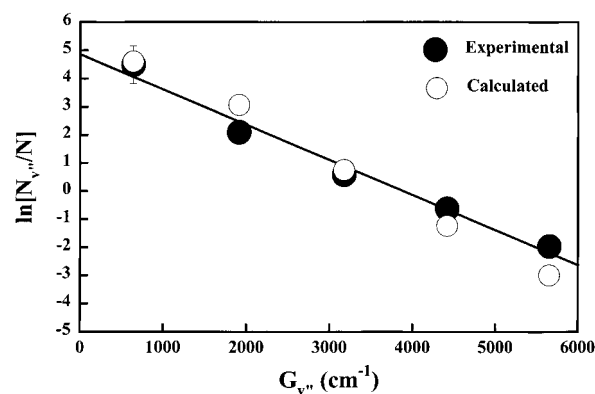

Figure 3. Observed vibrational state distribution of the CS(X$^1\Sigma^-$) product (●) following the reaction of O(^{3}P) + CS$_2$. O(^{3}P) atoms are produced by the 355 nm photolysis of NO$_2$ (0.075 Torr) in the presence of CS$_2$ (0.085 Torr). The delay between the photolysis and the probe lasers is 2 μs, corresponding to ca. three gas kinetic collisions. The open symbols (○) are the best fit to the experimentally observed data using Franck−Condon/Golden Rule model (see Discussion).

the spectroscopic constants reported by Barrow and co-workers.[32,33] Our results are in good agreement with the nascent vibrational state distributions reported in the literature.[25,26] The other factor that we have to consider in the O(^{3}P) + CS$_2$ experiment is the overlap of the vibronic bands of the CS(A$^1\Pi$ − X$^1\Sigma^+$) transition with those of the SO(B$^3\Sigma^-$, v' − X$^3\Sigma^-$, v'') transition. The following CS(A$^1\Pi$ − X$^1\Sigma^+$) vibronic bands were obtained with detectable signal and minimum overlap: (2,0), (2,1), (2,2), (2,3). The vibrational bands terminating on the $v' = 2$ level of A$^1\Pi$ state enable us to obtain a vibrational state population distribution without having to correct for the differences in emission properties and filters. In this way, the vibrational state population distribution of CS(X$^1\Sigma^+$, $v'' = 0-4$) can be obtained by measuring the integrated areas of these bands and normalizing them by their respective Franck−Condon factors.[34] In these experiments, the reactant partial pressures are $P_{NO_2} = 75$ mTorr and $P_{CS_2} = 85$ mTorr, with a delay time of 2 μs between the photolysis and the probe lasers. This corresponds to ca. 3 hard sphere collisions prior to the detection of the LIF signal. The CS(X$^1\Sigma^+$) vibrational state population distribution measured under these conditions is not expected to undergo significant relaxation from its nascent partitioning. The CS(X$^1\Sigma^+$) vibrational state population distribution (see Figure 3) can be characterized as a Boltzmann distribution with a vibrational temperature of 1128 ± 141 K. We have also measured the CS(X$^1\Sigma^+$) vibrational state population distribution under the same pressure conditions but with a 10 μs delay time corresponding to ca. 16 hard sphere collisions following the initiation of the reaction. The observed vibrational distribution under these conditions gives an experimentally identical vibrational temperature of 1230 ± 155 K for the vibrational levels $v'' = 0-3$. Attempts to measure a complete vibrational state distribution at lower collision numbers were unsuccessful due to low signal-to-noise ratios with vibrational levels of smaller population.

B. Product Rotational State Distributions. Rotational state distribution of SO(X$^3\Sigma^-$) and CS(X$^1\Sigma^+$) following the reaction of O(^{3}P) + CS$_2$ has also been measured. For sulfur monoxide, product rotational state distributions have been obtained for $v'' = 0-4$. In the CS case, only $v'' = 0$ was able to be sufficiently rotationally resolved at low enough collision numbers to yield a reliable rotational state distribution. The details of the rotational state distribution measurements of each of the two products are given below.

1. SO(X$^3\Sigma^-$). Rotationally resolved spectra have been

TABLE 1: Rotational Temperatures of the Nascent SO($X^3\Sigma^-$) Product as a Function of Vibrational Level, v''

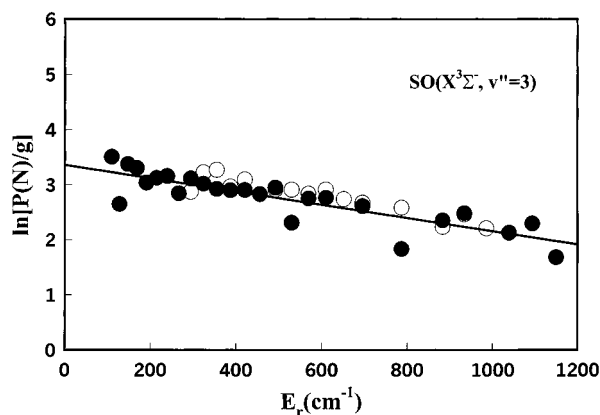| v''	0	1	2	3	4	5
T_r (K)	1172 ± 254	1312 ± 244	1017 ± 98	1121 ± 130	882 ± 180	707 ± 154

Figure 4. Boltzmann plots of the nascent rotational state distribution of SO($X^3\Sigma^-$, $v'' = 3$) products following the O(^{3}P) + CS$_2$ reaction after 1.5 kinetic gas collisions, corrected by the rotational degeneracy $g(N'') = (2N'' + 1)$, versus the rotational energy, By, $N''(N'' + 1)$. The symbols (●) and (○) represent P22 and R22 rovibronic transitions, respectively. The solid line is linear least-squares fits to the experimental data.

Figure 5. Boltzmann plots of the nascent rotational state distribution of CS($X^1\Sigma^+$, $v'' = 0$) products after the O(^{3}P) + CS$_2$ reaction. NO$_2$/CS$_2$ = 35/45 (mTorr). The delay between the photolysis and the probe lasers is 2 μs, corresponding to two gas kinetic collisions. The solid line is linear least-squares fits to the experimental data.

recorded on the SO($B^3\Sigma^- - X^3\Sigma^-$) transition for the ($v' = 1$, $v'' = n$) vibronic bands for $n = 0-4$ under conditions of 1.5 gas kinetic collisions. These rovibronic transitions originated from SO($X^3\Sigma^-$) have been used to measure the rotational state population distribution. Each rotational level of the $X^3\Sigma^-$ electronic state, which belongs to Hund's case b, is split into three spin components, that is, F$_1$ for $J = N + 1$, F$_2$ for $J = N$, and F$_3$ for $J = N - 1$, where N is the total quantum number without spin. Of these SO($B^3\Sigma^-$, $v' - X^3\Sigma^-$, v'') transitions, only six branches i.e., P$_{11}$, P$_{22}$, P$_{33}$, R$_{11}$, R$_{22}$, and R$_{33}$ have appreciable intensity. The frequencies corresponding to rovibronic transitions are calculated based on Colin's spectroscopic constants.[22,23] The experimental spectra were calibrated by adjusting the bandhead position to the calculated value. The assignment of each rovibronic transition was carried out by comparing the calibrated experimental spectra with the calculated lines. The difference between calculated rotational line positions and the experimental positions was within 0.005 nm. For the vibrational bands used, the P$_{22}$ and R$_{22}$ branches can be well-resolved. Typically, the R$_{22}$ branch can be assigned up to ca. $N = 40$ and P$_{22}$ branch up to ca. $N = 35$.

Relative rotational state populations are determined by measuring the intensity of each well-resolved line from the band, dividing by the appropriate line strength, i.e., Hönl–London factor, and multiplying by the corresponding rotational degeneracy. The rotational population, P(N''), measured from the LIF excitation spectra can be described approximately by a Boltzmann expression and thus characterized by a rotational temperature, T_r. The Boltzmann plots and resulting rotational temperatures are shown in Figure 4 and Table 1, respectively.

2. CS($X^1\Sigma^+$). For the CS($A^1\Pi - X^1\Sigma^+$) transition, attempts to get rotationally resolved spectra on the bands used for the vibrational state distribution under single collision conditions were unsuccessful due to low signal-to-noise ratios. This is due to relatively small Franck–Condon factors for the (2,0) band and the low populations found in the higher vibrational levels. Because of the vertical nature of the CS($A^1\Pi - X^1\Sigma^+$) transition, the (0,0) band has the largest Franck–Condon factor for the $v'' = 0$ level, where the relative nascent population from
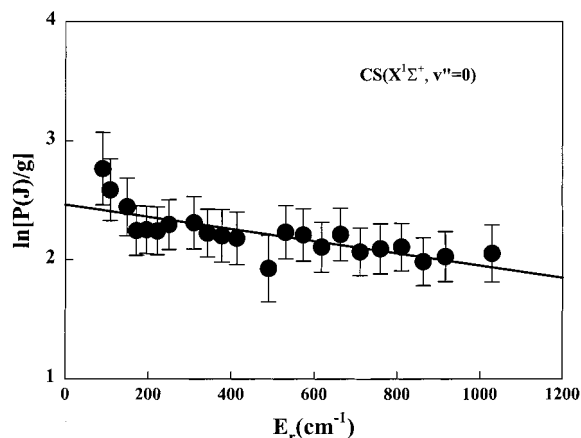
the reaction is the highest. Therefore, we have chosen to use the (0,0) band to record a rotationally resolved spectrum, which in turn can be converted into a rotational state distribution. The spectrum was obtained at partial pressures of $P_{NO_2} = 75$ mTorr and $P_{CS_2} = 85$ mTorr and a delay time of 2 μs, corresponding to three hard sphere collisions. While the CS rotational state distribution may be partially relaxed under these conditions, it is as close to nascent as we can directly measure. In the CS(0,0) band, the R branch which forms the bandhead at $\lambda = 257.55$ nm cannot be resolved, and the P branch is partially overlapped by the SO(3,4) band. However, the Q branch can be assigned unambiguously up to $J = 35$ (see Figure 1b). Transition frequencies are calculated based on the spectroscopic constants of Barrow and co-workers.[32,33] Following the assignment, rotational state populations were extracted by the same procedure used for the SO spectra. The CS($v'' = 0$) product rotational state distribution can be characterized as Boltzmann (see Figure 5) with a rotational temperature of 2986 ± 607 K. For the $v'' = 1, 2$ levels, due to the lower populations and smaller Franck–Condon factors of the CS(2,1) and (2,2) bands, rotational state distributions can be obtained following five gas kinetic collisions, with $T_r = 1310 \pm 169$ and 1166 ± 175 K, respectively. This rapid rotational relaxation is consistent with previously observed diatomic rotational relaxation.
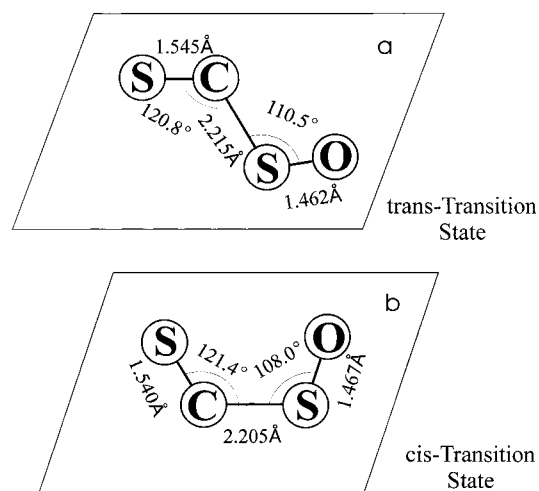
C. Theoretical Results. We obtained minimum energy structures corresponding to *trans*-OSCS and *cis*-OSCS complexes in the potential energy surfaces. Table 2 and Figure 6 show the ab initio energies and G-2 theoretical energy corrections of the species involved in the reaction. Figures 7 and 8 show the optimized geometries for intermediate complexes and transition states. Table 3 shows the calculated harmonic frequencies for each complex.

IV. Discussion

The experimental value for the heat of reaction for O(^{3}P) + CS$_2$ → CS + SO is $\Delta H_{RXN} = -84.46 \pm 3.76$ kJ mol^{-1}.[35,36] The uncertainties in the ΔH_{RXN} are purely from ΔH_f^0 at 298 K for CS. In the current study, we use the value of Douglas and Armentrout,[35] who reported one of the more precise values. The

Dynamics of the O(^{3}P) + CS$_2$(X$^1\Sigma_g^+$) Reaction

J. Phys. Chem. A, Vol. 105, No. 15, 2001 **3697**

TABLE 2: Complete Fourth-Order Møller−Plesset Energies (MP4 SDTQ/6-311++G*) and G-2 Theoretical Corrections for the Species Involved in the Title Reaction (in a.u)
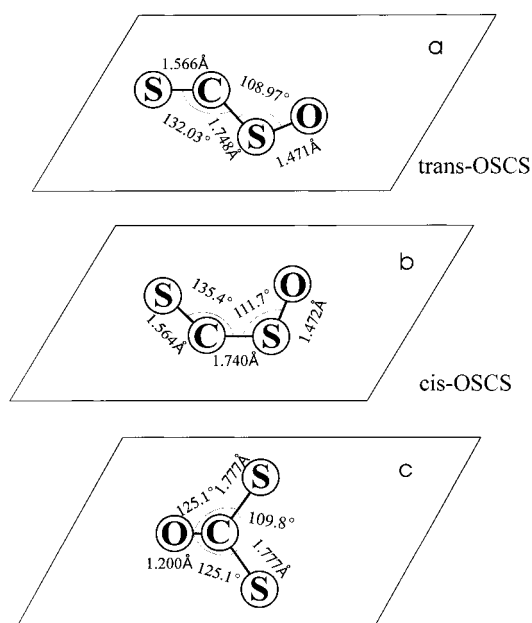
	MP4/6-311++G*	ΔE(2df)	ΔE(QCI)	ΔE(HLC)	ΔE(ZPE)	1.14npair	Δ	E$_0$(G$_2$)
O(^{3}P)	-74.937240	-0.03119	-0.00096	-0.01266	0	0.00228	-0.00239	-74.9821522
CS$_2$ ($^1\Sigma_g$)	-833.384280	-0.11515	0.007686	-0.04912	0.006978	0.00912	-0.00814	-833.532900
trans-OSCS	-908.322794	-0.16876	-0.00336	-0.06178	0.008813	0.0114	-0.01458	-908.551062
cis-OSCS	-908.3244281	-0.16854	-0.00304	-0.06178	0.009022	0.0114	-0.01440	-908.55177353
O=C〈^S_S	-908.376186	-0.1526738	- .023369	-0.06178	-0.008929	0.0114	-0.0121623	-908.605842
SO($^3\Sigma^-$)	-472.706690	-0.09609	0.002559	-0.03108	0.002504	0.0057	-0.00743	-472.830533
CS($^1\Sigma^+$)	-435.626792	-0.06053	0.002693	-0.03070	0.003015	0.0057	-0.00496	-435.711482
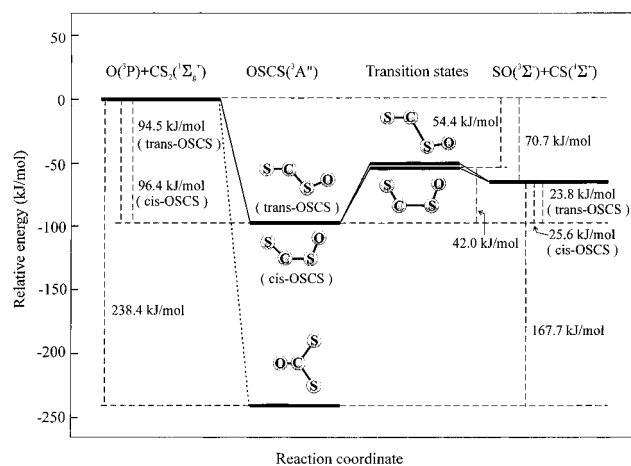
Figure 6. Energy level diagram for the O(^{3}P) + CS2 (X$^1\Sigma^-$) potential energy surface showing the minima and saddle points computed at the G2 level of theory. The *trans*-OSCS and *cis*-OSCS intermediate structures are nearly isoenergetic.

Figure 7. Optimized geometries of intermediate complexes obtained at the MP2/6-311++G* level of theory.

activation barrier for this reaction is 420 ± 24.5 cm^{-1}.[11,12] The center of mass kinetic energy of the O(^{3}P) atom following 355 nm NO$_2$ photolysis[37] corresponding to NO(X$^2\Pi$, $v = 0$) and to NO(X$^2\Pi$, $v = 1$) is 1833 and 610 cm^{-1}, respectively. Thus,

Figure 8. Optimized geometries of transition states obtained at the MP2/6-311++G* level of theory.

TABLE 3: Harmonic Frequencies for the OSCS Complex Determined at the MP2 Level of the Theory (in cm^{-1})

mode	ω_1	ω_2	ω_3	ω_4	ω_5	ω_6
trans-OSCS	163.54	198.33	374.98	568.05	1213.98	1349.56
cis-OSCS	155.4	253.7	472.5	529.8	1246.6	1302.2

oxygen atoms from both levels will have enough energy to allow the reaction to proceed over the activation barrier to products. The population of O(^{3}P) atoms produced from this photodissociation process corresponding to NO(X$^2\Pi$, $v = 0$) is 62 ± 3% and to NO(X$^2\Pi$, $v = 1$) is 38 ± 3%.[37] Therefore, the average kinetic energy of oxygen atoms will be 1368.0 ± 41.3 cm^{-1}, and the total available energy in reaction channel 1a is 8420.0 ± 355.6 cm^{-1}, which is available to be partitioned among all the products' degrees of freedom. While the other two channels (1b and 1c) are more exoergic, kinetic studies show that the reaction rate constants are much smaller and that the production of SO and CS is the primary pathway.[7,10,11]

The energies disposed to the SO(X$^3\Sigma^-$) and CS(X$^1\Sigma^+$) products' vibrational degrees of freedom in reaction la were obtained by summing the energy partitioned to each vibrational level, $E_{vib} = \Sigma C_v(E_v - E_0)$, where E_0 is the zero point energy, E_v is the vibrational energy in v'' levels, and C_v is the fractional population in v'' obtained from the vibrational state distributions (see Figures 2 and 3). The vibrational excitation for the SO(X$^3\Sigma^-$) product, obtained within two gas collisions was calculated to be 1531.5 ± 172.8 cm^{-1}, corresponding to 18.2% of the total available energy. The vibrational excitation for the CS(X$^1\Sigma^+$) product within ca. three collisions was 147.0 ± 18

3698 *J. Phys. Chem. A, Vol. 105, No. 15, 2001*

Cheng et al.

TABLE 4: Summary of the Energy Disposal into the SO(X$^3\Sigma^-$) and CS(X$^1\Sigma^-$) Products Following the O(^{3}P) + CS$_2$ Reaction

	CS(X$^1\Sigma^+$)		SO(X$^3\Sigma^-$)		SO(X$^3\Sigma^-$) and CS(X$^1\Sigma^+$)
	E_v	E_R	E_v	E_R	E_{trans}
energy (cm^{-1})	147.0	1930.0	1531.5	1002.2	
% E_{av}	1.8	22.9	18.2	11.9	35.8[a]

[a] Ref 17.

cm^{-1}, corresponding to 1.8% of E_{avail}. The total products' vibrational excitation accounts for 20.0% of the available energy.

The average rotational energy attributed to the products was calculated from $E_{rot} = \Sigma(k_B T_r C_v)/\Sigma C_v$, where k_B is the Boltzmann constant and T_r is the rotational temperature for each different vibrational level. For the SO(X$^3\Sigma^-$) product, where the rotational temperature can be obtained from $v'' = 0, 1, 2, 3, 4$ vibrational levels within two gas kinetic collisions, the temperatures are in the range of 882–1312 K. Thus, the calculated rotational energy is 1002.0 ± 132.1 cm^{-1}, corresponding to 11.9% of the total available energy. For the CS(X$^1\Sigma^+$) product, the rotational temperature can be obtained from the nascent CS($v'' = 0$) level as 2986 ± 607 K, while in the $v'' = 1, 2$ levels the temperatures are 1310 ± 169 and 1166 ± 175 K, respectively, under five collisions. The rotational energy calculated from these results for the CS product is 1930.0 ± 385.1 cm^{-1}, accounting for 22.92% of the available energy. The total rotational energy of the two products accounts for 34.8% of the available energy. The product translation accounts for 35.8% of the available energy.[17] On the basis of our results and those of ref 17, 90.6% of the available energy is partitioned among the translational, rotational, and vibrational degrees of freedom of the reaction products. A complete summary of the energy partitioning is given in Table 4.

The inverted vibrational distribution of the nascent SO(X$^3\Sigma^-$) suggests either a direct abstraction or the presence of a short-lived intermediate in the mechanism for reaction 1a. Reactive scattering results for the O(^{3}P) + CS$_2$ reaction shows sharp forward peaks, suggesting a weakly bound OSCS intermediate with a lifetime of one-third of a rotational period, based on a lifetime estimate of ~0.4 ps and a rotational period of ~1.3 ps.[17] We can estimate the lifetime of the intermediate by using quantum RRK theory[38] to calculate the unimolecular dissociation rate constant for the energized complex. The lifetime is the inverse of the rate constant: $\tau = 1/k_a$. Using an A factor of 10^{14} s^{-1}, we obtain a lifetime of 0.5 ps for the intermediate, assuming the energetics shown in Figure 6, in good agreement with the previous estimate.

The vibrational population distributions of SO(X$^3\Sigma^-$) and CS(X$^1\Sigma^+$) products following the title reaction can be treated by a Franck–Condon/Golden Rule model.[39] This model assumes a sudden transition from a dressed oscillator, i.e., the oscillators SO and CS, in the intermediate OSCS prior to dissociation, to the undressed diatomic reaction products SO and CS. We find that the best fit for the inverted vibrational state distribution of SO as shown in Figure 2 corresponds to a dressed SO oscillator with a bond length of 1.556 Å and a vibrational frequency of 1270 cm^{-1}. Application of this model to CS(X$^1\Sigma^+$) vibrational distribution reveals the bond length of the dressed CS in the intermediate prior to cleavage. The best fit of the calculated vibrational state distribution of CS(X$^1\Sigma^+$) is shown in Figure 3. The bond length of the dressed CS in the polyatomic intermediate is 1.570 Å.

The results of ab initio calculations of the intermediate complex OSCS on the ^{3}A″ potential energy surface may provide

a qualitative insight into the dynamics. The features on the calculated triplet-state potential energy surface provide an explanation for the nonstatistical behavior of the observed product state distributions. Upon formation of the transient intermediate OSCS, the system has at least 70 kJ/mol of excess energy. The S–C stretch requires about 42 kJ/mol for the *trans*- and *cis*-OSCS intermediates to dissociate to products. Since this is only 60% of the available energy, the transient complex can readily dissociate to SO + CS, leaving substantial energy in S–O vibration. Product formation via *trans*- and *cis*-OSCS intermediates are shown in Figure 7a,b. The bond length of the CS bond that does not break in the intermediates is averaged as 1.565 Å, which is the same as we obtained from the Franck–Condon/Golden Rule model (1.565 Å). In the parent molecule CS$_2$, the bond length is 1.55 Å. On the other side, the bond length of SO from the calculation is 1.471 Å (trans-), smaller than in FC/Golden Rule model, where it is 1.556 Å. The S–C–S angle decreases from 180° in the separated reactant to 132° (trans-) in the intermediate, consequently, if most of the available energy is repulsively released in the exit channel as the C–S bond breaks, and then a large lever arm will ensure substantial CS rotational excitation.

Smith[14] has shown experimentally that both CS and SO products in reaction 1a are vibrationally excited up to the third and fourth level and are characterized as Boltzmann distributions with vibrational temperatures of 1775 and 2870 K, respectively. Our results show that while the CS product is vibrationally excited up to $v'' = 4$ with a characteristic Boltzmann ($T_{vib} = 1128$ K) vibrational distribution, the SO product displays an inversion in its vibrational distribution. In Smith's experiment, he measured the CS distribution more precisely than he did SO, because the now accepted spectroscopy of sulfur monoxide was not available to him. His data were also recorded at much higher collision numbers than those reported here. The CS product vibrational distributions are similar, with the primary difference being that the vibrational temperature we obtained is lower than his result. However, he measured a Boltzmann temperature using only the $v'' = 0, 1, 2$ levels. If he had included this $v'' = 3$ point in temperature determination, he would have obtained a lower value.

The highly excited rotational degrees of freedom in the CS product suggest that the intermediate should not be linear. If the system is nearly collinear in the exit channel as repulsive forces push the products apart, the product will on average be created with little rotational momentum. Our ab initio calculation shows that the original linear CS$_2$ molecule bends nearly 130° in both the cis and trans planar intermediate structures and has a still tighter transition state structure. The reactive scattering experiments of Grice and co-workers[17] are in agreement on this point. It is interesting to compare the dynamics study results between reaction 1a and

$$O(^3P) + OCS \rightarrow CO + SO \qquad (2)$$
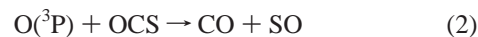
These two reactions are analogous to each other, both being reactions of O(^{3}P) atoms with similar triatomic, linear sulfides. Nickolaisen et al.[40] obtained CO(v'',J) product state distributions from reaction 2, with the CO product having little vibrational excitation. The vibrational branching ratio was found to be [$v'' = 1$]/[$v'' = 0$] ≈ 0.05, with CO($v'' \geq 2$) not detected. In contrast, the carbon monoxide rotational degrees of freedom are much hotter, with a nascent CO ($v'' = 0$) rotational distribution temperature of 4400 ± 390 K. In this study of reaction 2, the total CO internal excitation accounted for 16% of the available energy to products. Our results for the energy

Dynamics of the O(^{3}P) + CS$_2$(X$^1\Sigma_g^+$) Reaction

J. Phys. Chem. A, Vol. 105, No. 15, 2001 **3699**

disposal into the CS product following 1a are similar. The vibrational distribution of CS is a little more excited than CO with detectable signal until $v'' = 3$, and the rotational degrees of freedom of CS are hotter as well, leading to total CS internal excitation of 25.7% of the available energy. The SO product state distribution following reaction 2 studied earlier in our lab shows high vibrational excitation with detectable population up to $v'' = 9$ and inverted at $v'' = 5$.[24] The nascent SO product rotational temperature was found to be ca. 2300 K, accounting for 34% of the available energy to products. The SO product internal degrees of freedom are observed to be slightly less excited following reaction 1a, with vibrational excitation up to $v'' = 6$, an inversion at $v'' = 1$, and a nascent rotational temperature near 1300 K. Thus the total internal energy of SO accounts for 30% of the available energy following reaction 1a. Kinetic studies show that although reaction 1a is considerably less exothermic than reaction 2, i.e., $\Delta H° = -7052$ cm^{-1} as compared to $-17\,670$ cm^{-1}, it is much faster with a smaller activation barrier. One possible explanation is that the larger activation energy of reaction 2 is a reflection of the fact that the product CO is more difficult to excite than CS. This should show up qualitatively as a larger potential energy of interaction in the approach of O to OCS than to CS$_2$ or a greater activation energy, since less of the available energy was used up in CO excitation, i.e., CS internal excitation accounts for 25.7%, as compared to 16% in CO product in the comparison of the two channels.

Reactive scattering studies of these two reactions show that the center-of-mass angular distribution of SO for O + OCS is cone-shaped, peaking at a scattering angle $\theta \sim 70°$ with respect to the incident O atom direction, while that for O + CS$_2$ peaks sharply in the forward direction $\theta \sim 0°$.[17] The very fact that the angular distribution of the product is highly anisotropic implies that there is no long-lived OSCS or OSCO intermediate "complex", with OSCS being even shorter-lived. If the reaction duration were long as compared with the period of rotation of such an intermediate (i.e., several picoseconds), all memory of the initial directions would be lost and the angular distribution would have a forward−backward symmetry.[41] This is not the case for the two reactions. Indeed, if there were a long-lived intermediate, we would not expect a very specific energy disposal, since then there would be time for the energy disposal to be "equipartitioned" among the different modes. Grice and co-workers provide a mechanism arguing that the cone-shaped scattering for O + OCS arises from direct dissociation of the early transition state that is formed by broadside approach of the O atom to the S atom of the OCS molecule. The sideway recoil of the SO product is carried into the forward hemisphere by the initial momentum of the O atom. The forward peaked scattering for O + CS$_2$ arises from the precession of a weakly bound OSCS intermediate with a lifetime of one-third of a rotational period. In both cases, reaction occurs along a ^{3}A″ potential energy surface involving planar bent cis or trans intermediates (Figure 7) with bending mode excitation resulting in high product rotational excitation. Their mechanism is consistent with our experimental results, namely, both CS and CO are highly rotationally excited, and CS is a little more vibrationally excited than CO.

For the sake of completeness, we have calculated the intermediate shown in Figure 7c, even though we believe it is not involved in the formation of the SO and CS products. This structure has been calculated previously by Hershberger and co-workers[7] and agrees well with our works. Most likely, the structure shown in Figure 7c leads to the products shown in reactions 1b and 1c.

V. Summary

The carbon monosulfide (SO) and sulfur monoxide (SO) radicals were generated by laser photodissociation of NO$_2$ in the presence of CS$_2$. The rovibrational state distributions of SO(X$^3\Sigma^-$) and CS(X$^1\Sigma^+$) have been measured by using laser induced fluorescence spectroscopy on the SO(B$^3\Sigma^- \leftarrow$ X$^3\Sigma^-$) and CS(A$^1\Pi \leftarrow$ X$^1\Sigma^+$) transitions, respectively. Relative population of SO(X$^3\Sigma^-$) in $v'' = 0-6$ vibrational levels were determined from the normalized integrated intensities of the (1,0), (1,1), (1,2), (1,3), (1,4), (1,5), and (1,6) bands. The SO(X$^3\Sigma^-$) product is highly vibrationally excited, and the vibrational state distribution is inverted at $v'' = 1$ with detectable population up to $v'' = 6$. Relative concentrations of CS(X$^1\Sigma^+$) in $v'' = 0-3$ levels were determined from measurements on the (2,0), (2,1), (2,2), and (2,3) vibrational bands. The CS(X$^3\Sigma^+$) product vibrational state population distribution has been found to be a Boltzmann distribution with a vibrational temperature of 1230 K. The total vibrational excitation of the products accounts for 21% of the available energy to the products.

The near nascent CS($v'' = 0$) rotational distribution is characterized by a rotational temperature of $T_R = 2986$ K, and the near nascent SO($v'' = 1$) is characterized by a temperature of 1312 K. The total rotational energy of the two products accounts for 34.8% of the available energy.[18] The product translation accounts for 35.8% of the available energy. Thus the available energy is balanced to 91.6% in partitioning among the translational, rotational, and vibrational degrees of freedom of the reaction products.

Ab initio calculations of the OSCS complex on the ground state ^{3}A″ potential energy surface provide a qualitative insight into the dynamics. The observed vibrational state distributions have been modeled by Franck−Condon/Golden Rule treatment. Franck−Condon model best fits observed vibrational state distributions when the SO bond length is 1.556 Å and the CS bond length is 1.565 Å, which are in reasonable agreement with the minimum energy intermediate structures.

References and Notes

(1) Wayne, R. P. *Chemistry of Atmosphere*; Oxford University Press: Oxford, 1991.

(2) Warneck, P. *Chemistry of Natural Atmosphere*; Academic Press: New York, 1988.

(3) Levine, J. S. *The Photochemistry of Atmospheres*; Academic Press: New York, 1985.

(4) Tyndall, G. S.; Ravishankara, A. R. *Int. J. Chem. Kinet.* **1991**, *23*, 483.

(5) (a) Brown, S. D.; Ismail, K.; Thomas, K. M. *Energy Fuels* **1995**, *9*, 1104. (b) Farago, Z. *Combust. Sci. Technol.* **1991**, *79*, 73.

(6) Liu, K.; Wager, A. *The Chemical Dynamics and Kinetics of Small Radicals*; World Scientific Publishing Co. Pte. Ltd.: River Edge, NJ, 1995.

(7) Cooper, W. F.; Hershberger, J. F. *J. Phys. Chem.* **1992**, *96*, 5405.

(8) Smith, I. W. M. *Trans. Faraday Soc.* **1971**, *67*, 2586.

(9) Suart, R. D.; Dawson, P. H.; Kimbell, G. H. *J. Appl. Phys.* **1972**, *43*, 1022.

(10) Slagle, I. R.; Gilbert, J. R.; Gutman, D. *J. Chem. Phys.* **1974**, *61*, 704.

(11) Hsu, D. S. Y.; Shaub, W. M., Burks, T. L.; Lin, M. C. *Chem. Phys.* **1974**, *44*, 143.

(12) Westenberg, A. A.; deHaas, N. *J. Chem. Phys.* **1969**, *50*, 707.

(13) Wei, C. N.; Timmons, R. B. *J. Chem. Phys.* **1975**, *62*, 3240.

(14) Smith, I. W. M. *Faraday Soc. Discuss.* **1967**, *43−44*, 194.

(15) Geddes, J.; Clough, P. N.; Moore, P. L. *J Chem. Phys.* **1974**, *61*, 2145.

(16) Gorry, P. A.; Nowikow, C. V.; Grice, R. *Mol. Phys.* **1979**, *37*, 329.

(17) Rochford, J. J.; Powell, L. J.; Grice, R. *J. Phys. Chem.* **1995**, 15369.

(18) Chen, X.; Asmar, F.; Wang, H.; Weiner, B. R. *J Phys. Chem.* **1991**, *95*, 6415.

(19) Wang, H.; Chen, X.; Weiner, B. R. *J. Phys. Chem.* **1993**, *97*, 12260.

(20) Wang, H.; Chen, X.; Weiner, B. R. *Chem. Phys. Lett.* **1993**, *216*, 537.

(21) Frisch, M. J.; Trucks, G. W.; Schlegel, H. B.; Gill, P. M. W.; Johnson, B. G.; Robb, M. A.; Cheeseman, J. R.; Keith, T. A.; Petersson, G. A.; Montgomery, J. A.; Raghavachari, K.; Al-Laham, M. A.; Zakraewski, V. G.; Ortiz, J. V.; Foresman, J. B.; Cioslowski, J.; Stefanov, B. B.; Nanayakara, A.; Challacombe, M.; Peng, C. Y.; Ayala, P. Y.; Chen, W.; Wong, M. W.; Andres, J. L.; Replogle, E. S.; Gomperts, R.; Martin, R. L.; Fox, D. J.; Binkley, J. S.; Defrees, D. J.; Baker, J.; Stewart, J. P.; Head-Gordon, M.; Gonzalez, C.; and Pople, J. A. *Gaussian 94 (Revision A.)*, Gaussian, Inc., Pittsburgh, PA, 1995.

(22) Pople, J. A.; Head-Gordon, M.; Fox, D. J.; Raghavachari, K.; Curtiss, L. A. *J. Chem. Phys.* **1989**, *90,* 5622.

(23) Curtiss, L. A.; Raghavachari, K.; Trucks, G. W.; Pople, J. A. *J. Chem. Phys.* **1991**, *94,* 7221.

(24) Chen, X.; Wu, F.; Weiner, B. R. *Chem. Phys. Lett.* **1995**, *247*, 313.

(25) Butler, J. E.; Drozdoski, W. S.; McDonald, J. R. *Chem. Phys.* **1980**, *50*, 413.

(26) Yang, S. C.; Freedman, A.; Kawasaki, M.; Bersohn, R. *J. Chem. Phys.* **1980**, *72*, 4058.

(27) Dornhöfer, G.; Hack, W.; Lange, W. *J. Phys. Chem.* **1984**, *88*, 3060.

(28) Colin, R. *Can. J. Phys.* **1968**, *47*, 979.

(29) Colin, R. *J. Chem. Soc., Faraday Trans. 2* **1982**, *78*, 1139.

(30) Smith, W. H.; Liszt, H. S. *J. Quant. Spectrosc. Radiat. Transfer* **1975**, *11*, 45.

(31) We have measured some vibrational relaxation rates of SO (v''). Relaxation efficiencies range from ca. 10 collisions with near-resonant partners such as SO_2 to 10^4 collisions with noble gases, such as Ar and He.

(32) Lagerqvist, A.; Westerlund, H.; Wright, C. V.; Barrow, R. F. *Arkiv, För Fysik,* **1958**, *14*, 387.

(33) Barrow, R. F.; Dixon, R. N.; Lagerqvist, A.; Wright, C. V. *Ark. Fys.* **1960**, *18*, 543.

(34) Bergeman, T.; Cossart, D. *J. Mol. Spectrosc.* **1981**, *87*, 119.

(35) Douglas, A. P.; Armentrout, P. B. *J. Chem. Phys.* **1991**, *94*, 3563.

(36) Lide, D. R.; Kehiaian, H. V. *CRC Handbook of Thermophysical and Thermochemical Data*, CRC Press: Boca Raton, FL, 1994.

(37) Harrison, J. A.; Yang, X.; Felder, P.; Huber, J. R. *J. Phys. Chem.* **1994**, *98*, 12260.

(38) Robinson, P. J.; Holbrook, K. A. *Unimolecular Reactions*, Wiley-Interscience: A division of John Wiley & Sons Ltd., New York, 1972.

(39) Berry, M. J. *Chem. Phys. Lett.* **1974**, *29*, 323.

(40) Nickolaisen, S. L.; Veney, D. W.; Cartland, H. E. *J. Chem. Phys.* **1994**, *100*, 4926.

(41) Levine, R. D.; Bernstein, R. B., *Molecular Reaction Dynamics and Chemical Reactivity*, Oxford University Press: New York, 1987.